CHAPTER 6

PREPARATION AND CHARACTERIZATION OF ELECTRON BEAM EVAPORATED $LIMn_2O_4$, $LiNd_{0.05}Mn_{1.95}O_4$ AND $LiSm_{0.05}Mn_{1.95}O_4$ THIN FILMS

6.1 SCOPE OF THE CHAPTER

The miniaturization of Power sources is highly anticipated to keep pace with the advancement in the electronics industries. Lithium ion based Micro batteries have been identified as compatible power sources especially for Silicon based MEMS components. Though the technology has yielded few commercial products, the state of art of the technology still lies in the R&D level. The serious impediments in full fledged commercialization of this technology are the lower shelf life and higher initial cost. Among several factors responsible for lower shelf life, the impedance built up in the interface between electrode and electrolyte plays a major role and the selection of the suitable materials would be one of the possible solution for this.

Most of the Li ion solid state micro batteries utilize $LiCoO_2$ as its electrode because of its higher energy density in spite of its toxic nature, high cost and the practical limitation in complete delithiation. At present several electrodes are being investigated as an alternative to $LiCoO_2$, of which $LiMn_2O_4$ has attracted great deal of attention due to its low cost, ease preparative procedure and higher lithiation limit than $LiCoO_2$.

In order to obtain efficient performance, the thin film electrodes are expected to possess certain qualities viz., correct stochiometry, Good

crystallinity and excellent adherence to the substrate. Many efforts have been pursued and reported in the fabrication of thin film electrodes using various deposition techniques like Electron-beam evaporation, RF magnetron sputtering, Pulsed laser deposition, Chemical vapour deposition etc. (Bates 1993, Rougier 1998, Fragnaud 1995). The RF-sputtering method has attracted great deal of attention due to the reproducibility of thin films with good adherence. However, the need for high vacuum arrangement, Inert gases and high purity cum high density target material makes it less viable. Due to which Electron beam deposition has emerged as an alternative for RF sputtering, since it doesn't need high voluminous electrode materials, high level vacuum equipments and so on. Moreover the main advantage of this method is the ability to add doping cations which occludes the capacity fading of $LiMn_2O_4$ (Shokoohi 1992). This chapter focus on the preparation of thin film of materials based on $LiMn_2O_4$ through Electron beam Evaporation.

6.2 PREPARATION OF $Li_{1+X}Mn_2O_4$ THIN FILM THROUGH ELECTRON BEAM EVAPORATION.

The $Li_{1+x}Mn_2O_4$ (x = 0.0, 0.05) has been prepared using Microwave assisted Co-Precipitation synthesis as detailed in the Chapter 5. The conditions for the preparation of thin films have been elaborately presented in Chapter 3. The thin films have been deposited over Poly crystalline Pt substrate. After prior cleaning and drying as discussed in Chapter 3, the substrates have been loaded in the vacuum chamber. Once the desired emission current is reached, the substrate has been exposed to evaporant source. The thickness and rate of deposition has been monitored using quartz crystal monitor and controlled by remote emission current controller. Once the required thickness is reached, the source shutter has been closed and emission current and applied voltage has been gradually reduced to zero. The coated films over platinum substrate have been subjected to annealing for

600˚C in the ambient atmosphere and the annealed films have been subjected to structural and electrochemical characterization.

6.2.1 Structural Characterization

The structural features of annealed thin film samples prepared from $LiMn_2O_4$ and $Li_{1.05}Mn_2O_4$ powder samples have been analyzed through X-ray diffraction and presented in Figure 6.1. The observed diffraction patterns could be indexed to a cubic unit cell with Fd3m space group and good concurrence has been obtained with JCPDS standard (file No. 47-1719) for $LiMn_2O_4$ powder. All the thin film samples have been observed to possess predominant (1 1 1) hkl orientation. However the lattice parameters of $LiMn_2O_4$ powder (8.2488 Å) and thin film (8.1305 Å) samples exhibits marked difference. A small impurity peak corresponding to Mn_2O_3 has also been observed in $LiMn_2O_4$ thin film sample and this may be due to the Lithium loss during the evaporation. Hence the necessity to compensate the Li loss has been observed to be mandatory.

In advent of this, sample with excess of 5% lithium has been prepared and evaporated. The XRD pattern of the thin film sample prepared from 5% excess Lithiated powder shown in Figure 6.1 shows no peaks corresponding to Mn_2O_3, thus the formation of Mn_2O_3 impurity has been avoided. The diffraction pattern of thin film sample has been observed to possess single phase $LiMn_2O_4$ with predominant orientation in (111) plane and the lattice parameter difference between powder $LiMn_2O_4$ (8.2488 Å), powder $Li_{1+x}Mn_2O_4$ (8.2533Å) and $Li_{1+x}Mn_2O_4$ Thin film sample (8.2475Å) has been observed to be very meagre. Moreover the unit cell dimensions of $Li_{1+x}Mn_2O_4$ thin film sample and $LiMn_2O_4$ bulk sample possess more resemblance. Hence it could be elucidated that the excess of lithium addition in the compound would compensate the lithium loss during thin film vapour deposition.

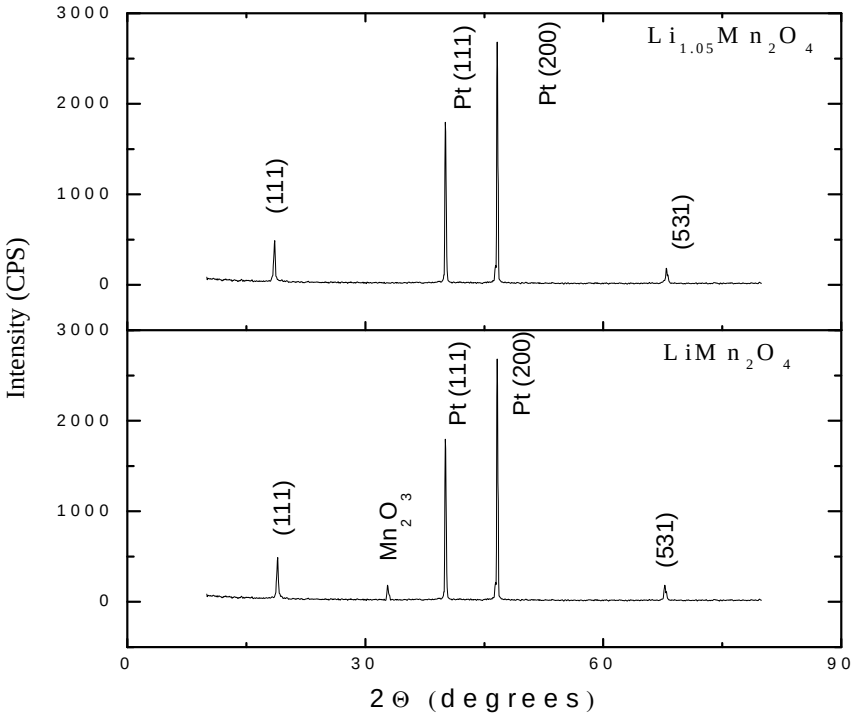

Figure 6.1 XRD pattern of $LiMn_2O_4$ and $Li_{1.05}Mn_2O_4$ thin film

The structural parameters of the thin film calculated from the diffraction pattern have been presented in Table 6.1. The Strain has been observed to increase with Li concentration in powder sample and which is obvious because of the excess Li occupancy in tetrahedral site, whereas in the case of thin films the strain has been observed to decrease with increasing Li concentration. The strain of thin film of $Li_{1.05}Mn_2O_4$ has been observed to be equal to that of $LiMn_2O_4$ powder, which entails the compensation of Lithium loss by excess lithium and the expected $LiMn_2O_4$ stochiometry of the thin film. The crystallite sizes of the samples have been calculated using Debye-Scherer formula. The crystallite sizes for both thin film samples have been observed to be in the order of 30 nm.

Table 6.1 Structural parameters of $LiMn_2O_4$ Powder and Thin films

Sample	FWHM	Lattice value (Å)	Crystallite Size (nm)	Strain ($lines^{-2}$ m^{-4})	Dislocation density ($lines.m^{-2}$)
$LiMn_2O_4$ (Powder)	0.2606	8.2488	32.250	0.06431	0.00096
$Li_{1.05}Mn_2O_4$ (Powder)	0.2997	8.2533	28.060	0.07392	0.00127
$LiMn_2O_4$ (Thin Film)	0.2717	8.13053	30.960	0.06699	0.00104
$Li_{1.05}Mn_2O_4$ (Thin Film)	0.2647	8.2475	31.560	0.06703	0.00100

6.2.2 Morphological Parameters

The scanning electron micrographs depicting the morphological features of the $Li_{1+x}Mn_2O_4$ (x = 0.0, 0.05) thin films have been shown in Figure 6.2. The micrographs have been subjected to image processing using 'Image-J' software (Image J 2002).

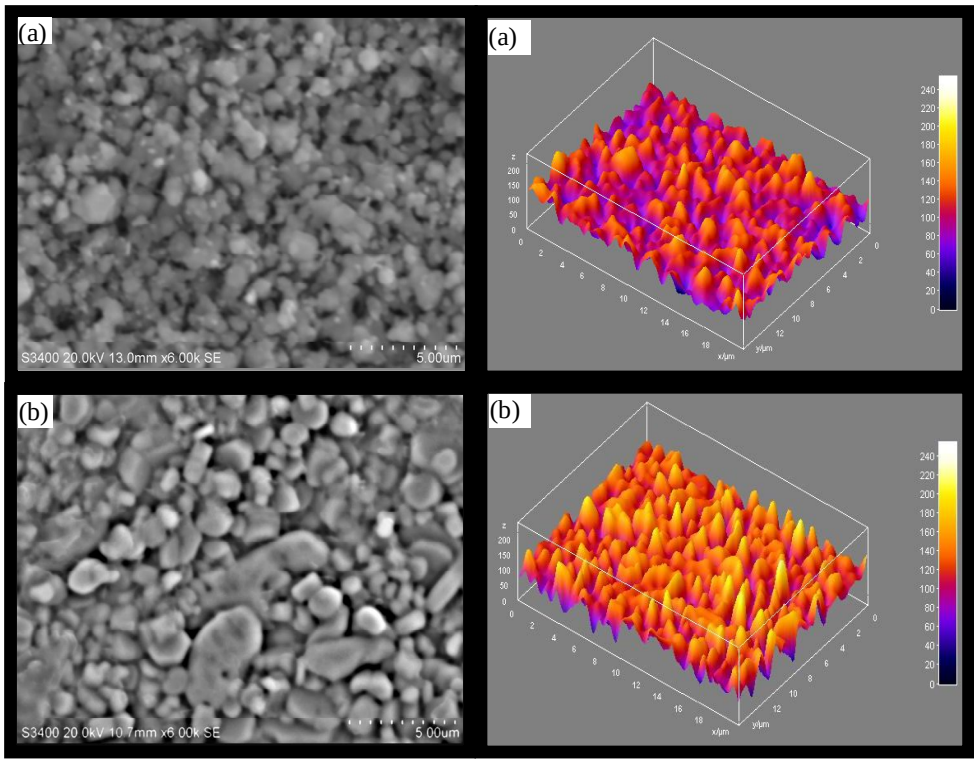

Figure 6.2 Scanning Electron Micrograph and 3D Topography of (a) $LiMn_2O_4$ (b) $Li_{1.05}Mn_2O_4$

The image processing have been carried out in four stages namely De-noising, Pore shape regularization, Binarisation and Quantification of relevant features to ascertain porosity, pore size distribution and surface texture. The de-noising has been carried out using Median filter and the pore shape regularization and binarisation has been carried out using 'BinariseSEM' Java plug-in provided in the software. The porosity, pore area, pore aspect ratio and grain size have been determined by using 'ComputeStats' Java plug-in provided in the software (ImageJ 2002). The surface texture and the roughness have been computed using '3D' and 'Roughness calculation' Java plug-ins. The Table 6.2 shows the observed morphological parameters.

The porosity is considered to be one of the major properties in ascertaining the electrochemical properties. For higher porosity, the electrochemical active surface area is higher i.e., contact area between electrode end electrolyte is higher. Hence to obtain efficient electrode performance high surface area electrodes are generally preferred. From the Table 6.2, it could be observed that the porosity increases with increasing Lithium concentration and this may be due to the reduced grain size. The observed increase in pore aspect ratio (ratio between diameters of the pore to its depth) may be considered as positive effect because, as the pore aspect ratio increases, the contact area between electrolyte and the cathode increases and thereby the improved electrochemical performance could be achieved. The root mean square roughness increases with Li excess thin film and this is in accordance with the effect observed by Simmen et al (2007).

Table 6.2 Morphological Parameters of $LiMn_2O_4$ Thin Films

Sample	Grain Size (μm)	Pore Area $(\mu m)^2$	Pore Aspect ratio	Porosity	Pore size	Roughness (nm)	
						RMS	AM
$LiMn_2O_4$	0.708	23.207	1.632	0.377	20.455	106.654	102.324
$Li_{1.05}Mn_2O_4$	0.485	61.272	1.809	0.593	25.186	128.562	127.244

6.2.3 Electrochemical Studies

The Figure 6.3 shows the typical cyclic voltammograms of the thin film electrodes $Li_{1+x}Mn_2O_4$ (x = 0.0, 0.05) in non aqueous electrolyte. The Cyclic voltammogram has been carried out in very slow scan rate so as to attain complete reaction. The pattern of reversibility curve has been observed to be similar in both the samples, but the extent of peak splitting and the area between anodic and cathodic peaks are lower in the case of $LiMn_2O_4$ sample. This may be because of the inferior stochiometry of the sample and presence of Mn_2O_3 impurity. The insertion of Lithium into the $LiMn_2O_4$ crystal lattice has been known to occur in two stages as indicated in the equation (6.1) and (6.2)

$$\underset{\text{(cubicPhase II)}}{Li_{1-x}Mn_2O_4(0.4<x<0.8)} \rightarrow \underset{\text{(Cubic Phase I)}}{Li_{1-x}Mn_2O_4(0.05<0.4)} \quad (6.1)$$

$$\underset{\text{(Cubic Phase I)}}{Li_{1-x}Mn_2O_4(0.05<0.4)} \rightarrow \underset{\text{(Cubic Phase I)}}{LiMn_2O_4} \quad (6.2)$$

Apart from these two redox peaks for $LiMn_2O_4$ sample, an another set of redox peak around 3.75 V has been observed, which may be attributed to the unwanted phase transition taking place in the sample due to Li deficiency, Whereas for the $Li_{1.05}Mn_2O_4$ sample, the extra peak has been observed to absent and it be corroborated to the compensation of Li loss and maintenance of 1:2 Li/Mn ratio in the sample.

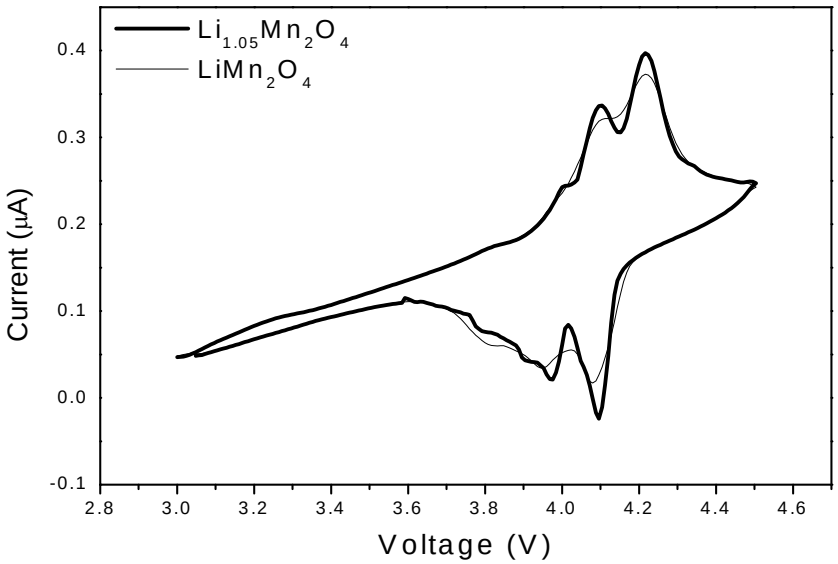

Figure 6.3 Cyclic Voltammetry of thin films of $LiMn_2O_4$ and $Li_{1.05}Mn_2O_4$

6.3 PREPARATION OF $LiNd_{0.05}Mn_{1.95}O_4$ AND $LiSm_{0.05}Mn_{1.95}O_4$ THIN FILMS

The Samples with Neodymium and Samarium dopants have been prepared with Li: Mn: Dopant in the ratio 1.05:1.95:0.05 using co-precipitation method. The 5% excess of lithium has been maintained in all the samples to compensate the Li loss during the evaporation while thin film fabrication. The concentrations of Li, Mn and dopant have been confirmed using ICP-AES analysis. The thin films of $LiNd_{0.05}Mn_{1.95}O_4$ and $LiSm_{0.05}Mn_{1.95}O_4$ have been deposited over Indium Tin oxide coated glass substrate using Electron beam Evaporation to the thickness of about 2 microns and annealed at 500°C for 3h in vacuum furnace. The annealed samples have been subjected to Structural, Morphological and Electrochemical characterization.

6.3.1 Structural Analysis

The results of structural analysis of the dopants have been presented in Figure 6.4. The XRD patterns of the thin films annealed at two different temperatures have been presented. The intensity of (1 1 1) peak corresponding to the compound has been observed to increase with increasing temperature, which entails the influence of annealing temperature in compound formation. The lattice values, strain associated with thin film and residual stress due to doping have been calculated and presented in Table 6.3. For both the Sm and Nd doped sample the peak corresponding to $InSnO_5$ has been observed around 31.2 degrees and whose intensity is higher than the intensity of the peaks corresponding to compounds. For the Sm doped sample, another extra peak around 12 degrees has been observed and this could be attributed to the In_2O_3 peak in the substrate and for higher annealing temperature the increment in intensity of the peak has also been observed.

500°C

Table 6.3 Structural Parameters of Thin film of $LiNd_{0.05}Mn_{1.95}O_4$ and $LiSm_{0.05}Mn_{1.95}O_4$ samples

Samples	Lattice Parameter (Å)	Strain ($lines^{-2}.m^{-4}$)	Dislocation Density ($x10^{-18}.lines.m^{-2}$)	Residual stress (Gpa)
$LiNd_{0.05}Mn_{1.95}O_4$ (350°C)	8.2855	0.043735	0.014567	3.84E-06
$LiNd_{0.05}Mn_{1.95}O_4$ (500°C)	8.2488	0.04393	0.014697	-4.2E-06
$LiSm_{0.05}Mn_{1.95}O_4$ (350°C)	8.2339	0.04401	0.01475	7.83E-06
$LiSm_{0.05}Mn_{1.95}O_4$ (500°C)	8.215	0.044111	0.014818	2.92E-06

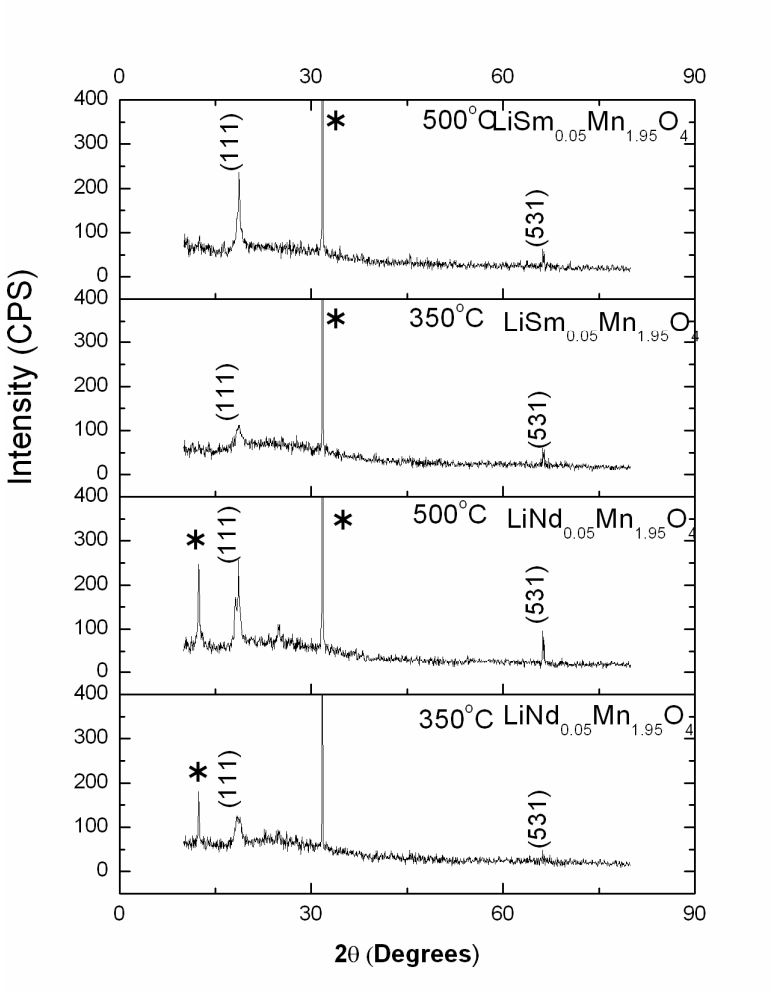

Figure 6.4 XRD pattern of $LiNd_{0.05}Mn_{1.95}O_4$ and $LiSm_{0.05}Mn_{1.95}O_4$ annealed at 350°C and 500°C

Other than (1 1 1) orientation, another orientation corresponding to (5 3 1) hkl direction has also been observed for all the samples. The increment intensity of both (1 1 1) and (5 3 1) peak with increasing annealing temperature shows the better compound formation in higher temperatures. The other parameters deduced from the structural data have been presented in Table 6.3. The strain and dislocation density has been observed to increase

with the increase in annealing temperature. The residual stress has been observed to change from compressive nature during annealing at low temperature to tensile nature during annealing at high temperature.

6.3.2 Morphological Parameters

The morphology of the samples obtained from scanning electron microscopy have been provided in the Figure 6.5. The morphological parameters obtained from the SEM have been given in Table 6.4. For both the samples, the grain size has been observed to increase due to annealing and also the grain aggregations have been observed in the micrograph. Due to the presence of aggregated grains, the enhancement in porosity with increasing annealing temperature has been observed. Since, the porosity, compound formation has improved with temperature the annealing of thin film to 500°C has been observed to be optimal (Xiang Ming Wu 2004). The surface roughness has been calculated from the 3D micrograph of the sample. The 3D topography of the surface of the thin film has been presented in Figure 6.6. The surface roughness has been observed to increase with increase in annealing temperature.

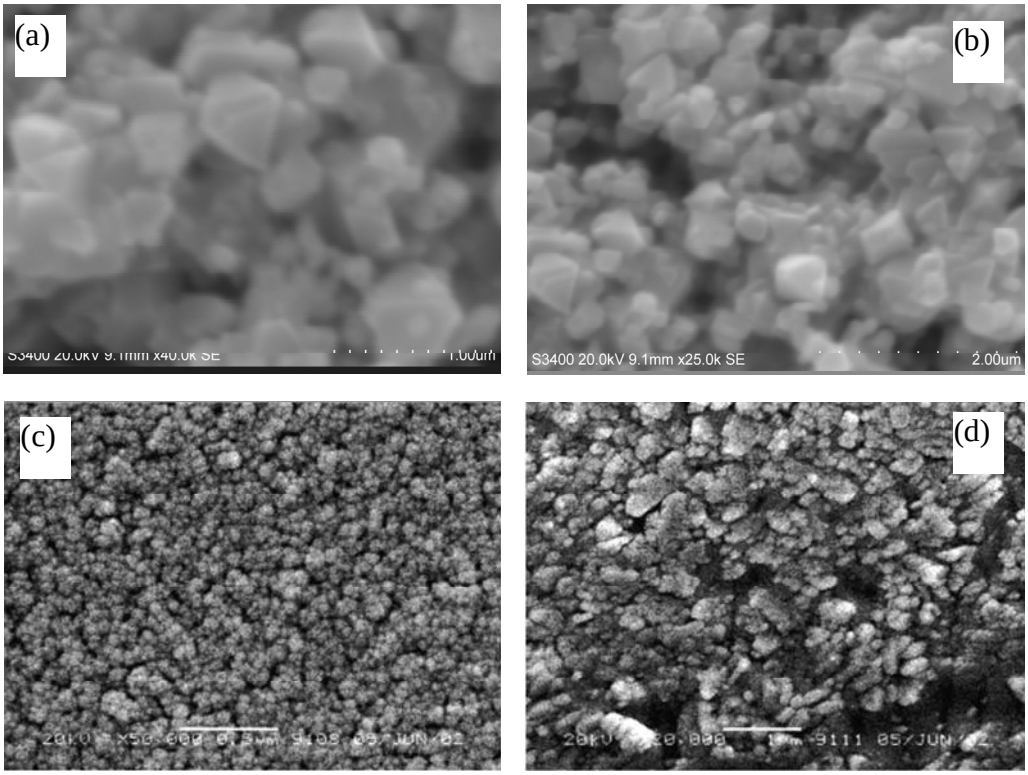

Figure 6.5 Scanning electron micrograph of thin films samples (a) 350°C (b) 500°C annealed $LiNd_{0.05}Mn_{1.95}O_4$; (c) 350°C (d) 500°C annealed $LiSm_{0.05}Mn_{1.95}O_4$

Table 6.4 Morphological parameters from SEM

Sample	Porosity	Area $(\mu m)^2$	Aspect ratio	Grain Size (µm)	Roughness (nm)	
					RMS	AM
$LiNd_{0.05}Mn_{1.95}O_4$	0.3021	0.001	1.703	0.4737	126.363	124.471
$LiNd_{0.05}Mn_{1.95}O_4$	0.5166	0.05814	1.688	0.4736	126.862	124.900
$LiSm_{0.05}Mn_{1.95}O_4$	0.2126	0.0275	1.718	0.1	126.464	124.013
$LiSm_{0.05}Mn_{1.95}O_4$	0.2344	0.0295	1.724	0.2043	132.769	129.763

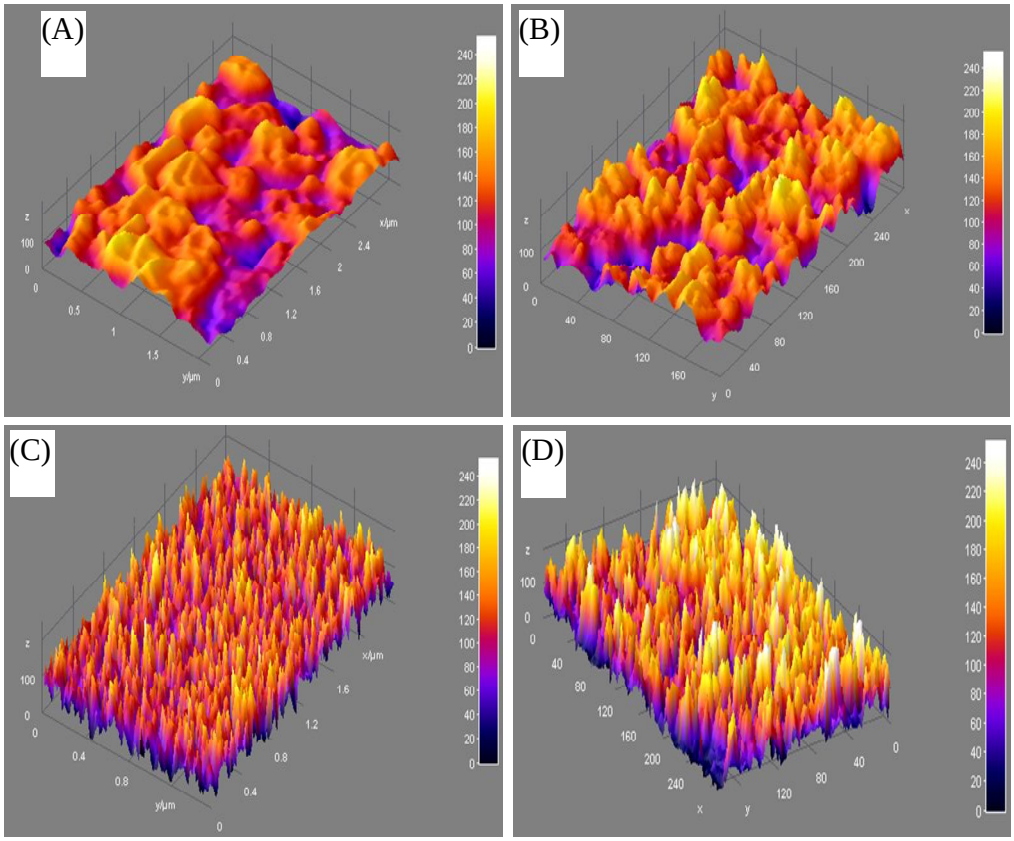

Figure 6.6 3D topography of thin films samples (a) 350°C (b) 500°C annealed $LiNd_{0.05}Mn_{1.95}O_4$; (c) 350°C (d) 500°C annealed $LiSm_{0.05}Mn_{1.95}O_4$

6.3.3 Electrochemical Properties

The cylic voltammetry of the $LiNd_{0.05}Mn_{1.95}O_4$ and $LiSm_{0.05}Mn_{1.95}O_4$. Thin film samples annealed at 500°C have been shown in Figure 6.7. Since the substrate used for the deposition is indium tin oxide coated glass substrate, the voltammentry curve possess only slight split in the anodic and cathodic peak. The observed peaks are in good concommitance with that of powder sample. The anodic and cathodic peaks of both the thin film samples have shown shift towards lower potential rather than the corresponding powders (Kang 2001).

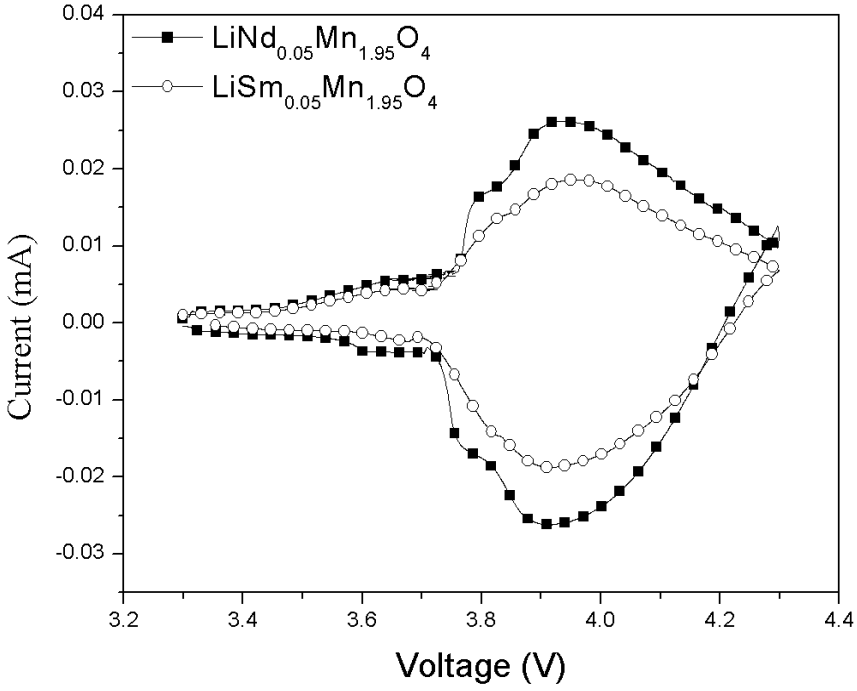

Figure 6.7 Cyclic Voltammetry of $LiNd_{0.05}Mn_{1.95}O_4$ and $LiSm_{0.05}Mn_{1.95}O_4$ thin films

6.3.4 Charge-Discharge Studies

The charge -discharge studies of the thin film samples have been carried out using chrono potentiometry. The galvanostatic cycling has been carried in C/5 rate and the corresponding discharge curves have been shown in Figure 6.8. The time taken for discharge of both the compounds has been identified to be identical. Since both the samples possess similar thickness and density, the capacity could be identified to be identical. Depending upon the mass of the deposit after annealing, the discharge capacity has been observed to be 109 μAh/g and 103 μAh/g for $LiNd_{0.05}Mn_{1.95}O_4$ and $LiSm_{0.05}Mn_{1.95}O_4$ respectively.

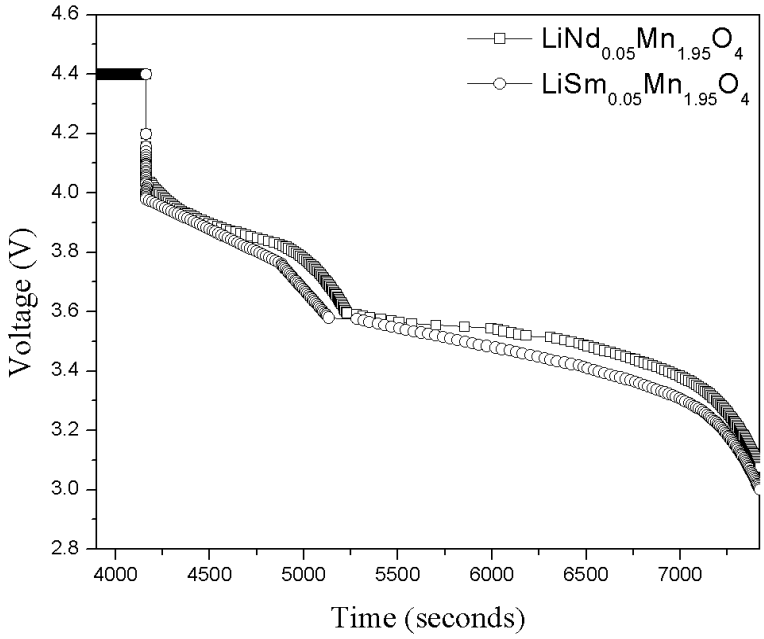

Figure 6.8 Chrono potentiometry curve of Thin film samples in C/5 rate

6.3.5 Cycle Life Studies

The cyclability of the both the thin film electrodes have been shown in Figure 6.9 respectively. In both, electrodes the decrease from the initial capacity has been observed and this may be due to the irreversible phase transition during deep discharge in the first cycle. But appreciable capacity retention has been observed for both the samples on further cycling. The capacity retention of Nd doped sample after 25 cycles has been observed to be around 81.65% and for Sm doped sample, the retention is around 83.0%. Thus the samarium doped samples have exhibited appreciable capacity retention and especially the capacity retention of both the thin film sample would be of greater interest in the field of Thin film Micro Batteries.

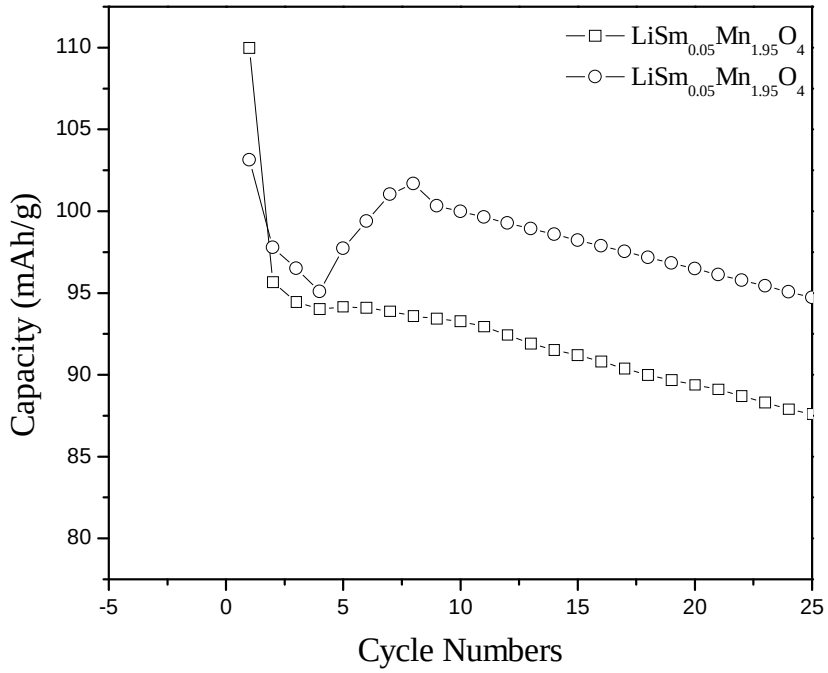

Figure 6.9 Cycle Life of the Thin film Samples